PHOTONICS Research

High energy soliton pulse generation by a magnetron-sputtering-deposition-grown $MoTe_2$ saturable absorber

Jintao Wang,[1,2] Zike Jiang,[1] Hao Chen,[1] Jiarong Li,[1] Jinde Yin,[1,2] Jinzhang Wang,[1] Tingchao He,[3] Peiguang Yan,[1,*] and Shuangchen Ruan[1]

[1]Shenzhen Key Laboratory of Laser Engineering, Key Laboratory of Advanced Optical Precision Manufacturing Technology of Guangdong Higher Education Institutes, College of Optoelectronic Engineering, Shenzhen University, Shenzhen 518060, China
[2]Key Laboratory of Optoelectronic Devices and Systems of Ministry of Education and Guangdong Province, College of Optoelectronic Engineering, Shenzhen University, Shenzhen 518060, China
[3]College of Physics and Energy, Shenzhen University, Shenzhen 518060, China
*Corresponding author: yanpg@szu.edu.cn

Received 22 January 2018; revised 18 March 2018; accepted 22 March 2018; posted 23 March 2018 (Doc. ID 320274); published 30 April 2018

The pulse energy in the ultrafast soliton fiber laser oscillators is usually limited by the well-known wave-breaking phenomenon owing to the absence of a desirable real saturable absorber (SA) with high power tolerance and large modulation depth. Here, we report a type of microfiber-based $MoTe_2$ SA fabricated by the magnetron-sputtering deposition (MSD) method. High-energy wave-breaking free soliton pulses were generated with pulse duration/pulse energy/average output power of 229 fs/2.14 nJ/57 mW in the 1.5 μm regime and 1.3 ps/13.8 nJ/212 mW in the 2 μm regime, respectively. To our knowledge, the generated soliton pulses at 1.5 μm had the shortest pulse duration and the highest output power among the reported erbium-doped fiber lasers mode locked by transition metal dichalcogenides. Moreover, this was the first demonstration of a $MoTe_2$-based SA in fiber lasers in the 2 μm regime, and the pulse energy/output power are the highest in the reported thulium-doped fiber lasers mode locked by two-dimensional materials. Our results suggest that a microfiber-based $MoTe_2$ SA could be used as an excellent photonic device for ultrafast pulse generation, and the MSD technique opens a promising route to produce a high-performance SA with high power tolerance and large modulation depth, which are beneficial for high-energy wave-breaking free pulse generation.

OCIS codes: (140.3510) Lasers, fiber; (140.4050) Mode-locked lasers; (140.7090) Ultrafast lasers; (160.4330) Nonlinear optical materials.

https://doi.org/10.1364/PRJ.6.000535

1. INTRODUCTION

High-power ultrafast pulses at 1.5 μm and 2 μm have attracted enormous attention in recent years because of their many important applications in materials processing, micromachining, medicine, metrology, and nonlinear optical conversion [1]. However, the energy of ultrafast pulses is generally limited by optical wave breaking, which is a consequence of excessive nonlinearity [2]. It has been demonstrated that a saturable absorber (SA) with a large modulation depth could suppress the wave-breaking effect and support ultrafast pulse generation with higher single pulse energy [3]. Therefore, an excellent SA with high power tolerance and large modulation depth was desired to realize high-power ultrafast pulse generation. Recently, different kinds of materials [e.g., carbon nanotubes, graphene, topological insulators, transition metal dichalcogenides (TMDs), and black phosphorus] [4–21] have been utilized as SAs. Among these SAs, TMDs possess outstanding position with the superior properties of non-zero band gap and layer-dependent third-order optical nonlinearity. $MoTe_2$, a new member of the TMDs, has a smaller direct band gap of about 1.1 eV (indirect gap of 1.0 eV in its bulk form) [22] compared with other TMDs (e.g., the direct band gaps of monolayer WS_2, MoS_2, WSe_2, and $MoSe_2$ are 2.1, 1.8, 1.65, and 1.57 eV, respectively) [1,23], making the $MoTe_2$-based SA more suitable in the near-infrared wavelength regime. Most recently, Mao *et al.* reported the nonlinear optical properties of few-layer $MoTe_2$ fabricated by a liquid exfoliation method, and achieved soliton mode-locking operations in an erbium-doped fiber (EDF) laser with pulse duration of 1.2 ps [17]. Bulk-structured WTe_2 microflakes as another counterpart were also demonstrated as a fast mode locker to achieve soliton pulse generation with pulse duration of 770 fs in the 1.5 μm regime [11].

Unfortunately, because the modulation depths of the SAs were 1.8% and 2.85% in the above two works, the reported output powers of the soliton pulses were limited to a small level of 0.04 mW. From this viewpoint, it is still challenging as to how to achieve high-energy soliton pulse generation by the state-of-the-art nanomaterial-based SAs.

In this paper, aiming to generate high-energy soliton pulses, we fabricated a type of $MoTe_2$ SA with high power tolerance and large modulation depth by the magnetron-sputtering deposition (MSD) method. The deposited $MoTe_2$ film covered tightly over the microfiber with a length of up to several centimeters. As a result, it could provide strong modulation of light in the laser cavity via evanescent wave interaction even at a high-power level, which is in favor of generating a high-energy pulse. The modulation depth of the $MoTe_2$ SA was measured to be 25.5% at 1.5 μm and 22.1% at 2 μm, respectively. By inserting the SA into the EDF and thulium-doped fiber (TDF) laser cavities, high-energy soliton pulses were demonstrated with pulse duration/pulse energy/average power of 229 fs/2.14 nJ/57 mW at 1.5 μm and 1.3 ps/13.8 nJ/212 mW at 2 μm, respectively. To our knowledge, the generated soliton pulses at 1.5 μm had the shortest pulse duration and the highest output power among the reported EDF lasers mode locked by TMDs. Moreover, this was the first demonstration of a $MoTe_2$-based SA in fiber lasers in the 2 μm regime, and the pulse energy and the output power are the highest in the reported TDF lasers mode locked by two-dimensional (2D) materials.

2. FABRICATION AND CHARACTERIZATION

The preparation process of the microfiber-based $MoTe_2$ SA is briefly explained as follows. First, the microfibers with effective fused zone length of about 1 cm and waist diameter of about 20 μm were obtained by stretching single-mode fibers (SMF-28e) on a taper drawing machine. Then, $MoTe_2$ film was deposited onto the waist of the microfibers by MSD technique. In brief, the microfibers and the $MoTe_2$ target with purity of 99.99% were placed into the vacuum chamber. The vacuum degree was pulled to 9×10^{-4} Pa by using a vacuum pump. After that, ionized Ar was excited to bombard the $MoTe_2$ target. The inspired $MoTe_2$ plasma plume was then deposited onto the microfibers gradually. During the depositing process, the microfibers were rotated with the speed of 20 r/min to ensure the uniformity of $MoTe_2$ film around the waist of the microfiber. The scanning electron microscopy (SEM) image of the as-prepared $MoTe_2$ SA was shown in Fig. 1(a). It can be seen that a compact layer of $MoTe_2$ film was indeed grown onto the whole microfiber. The SEM image of the cross section of the microfiber shown in Fig. 1(b) was utilized to detect the exact thickness and surface morphology of the $MoTe_2$ film coated on the microfiber. The magnified SEM image in the inset revealed that the thickness of the as-prepared $MoTe_2$ film was about 11.6 nm. The $MoTe_2$-coated areas were clearly seen from the scattered light by guiding a 650 nm visible light through the microfiber, as shown in Figs. 1(c) and 1(d). Figure 1(e) shows the field intensity of the guided mode in the microfiber. It can be seen that the energy has penetrated into the cladding in this case, which could efficiently decrease

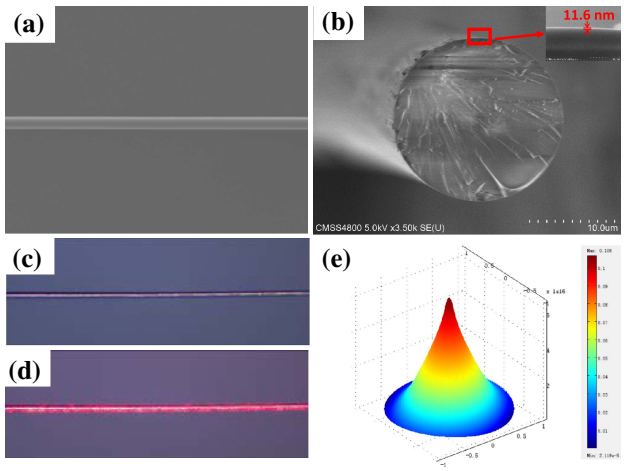

Fig. 1. (a) SEM image for microfiber coated with $MoTe_2$ film. (b) SEM image of the cross section of microfiber. The inset is a magnified SEM image. Optical microscope images of the waist region of sample (c) without and (d) with the guiding red light. (e) Field intensity of the guided mode in the microfiber.

average nonlinearity and is helpful for matter–light interaction through the evanescent wave-coupling effect.

X-ray photoelectron spectroscopy (XPS) was measured with an *in situ* XPS device (PHI 5000 VersaProbe II) to analyze the elemental composition and the bonding types of the prepared $MoTe_2$ film. Figure 2 presents XPS analysis of the $MoTe_2$. All spectra were calibrated by using the C 1s peak at 284.6 eV as a reference. Figure 2(a) shows the full spectrum of $MoTe_2$ film. As shown in Figs. 2(b) and 2(c), for the high-resolution Mo 3d and Te 3d spectra, the prominent Mo $3d_{5/2}$, Mo $3d_{3/2}$, Te $3d_{5/2}$, and Te $3d_{3/2}$ peaks appeared at 228.49, 231.87, 573.25, and 583.62 eV, respectively. The weak peaks of 232.99 eV and 236.12 eV in Fig. 2(b) correspond to Mo-O bonds, and 576.99 eV and 587.37 eV in Fig. 2(c) correspond

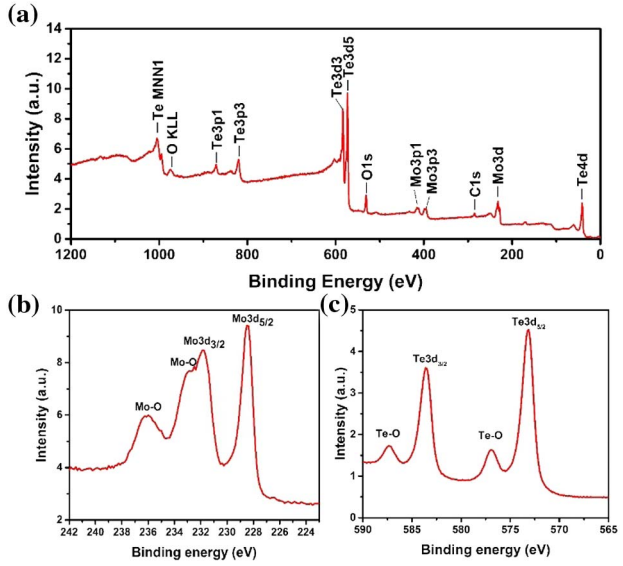

Fig. 2. (a) XPS spectrum of $MoTe_2$ film. (b) XPS core level spectrum of Mo 3d. (c) XPS core level spectrum of Te 3d.

to the Te-O bonds, respectively. The small shoulder peaks of Mo-O and Te-O may come from the oxidation products of $MoTe_2$ [24]. In this case, the small shoulder peaks indicated that the surface of the $MoTe_2$ film was slightly oxidized due to its air-sensitive properties and exposure to air [24]. The observed binding energies agree with the values measured over the years for the binding energies of Te 3d and Mo 3d [24,25]. The XPS spectra revealed the existence of Mo and Te core electron peaks, indicating that $MoTe_2$ film was indeed deposited on the microfiber.

In order to investigate the linear transmission of $MoTe_2$ film, the $MoTe_2$ film was also prepared with the same grown conditions as the one fabricated on the microfiber. The linear transmission of the prepared $MoTe_2$ film grown on Al_2O_3 substrate was measured from 1000 nm to 2000 nm with a spectrometer (Lambda 950). As shown in Fig. 3(a), it had an average transmission of 73.4%@1550 nm and 77.6% @1900 nm. The linear transmissions of the fabricated absorber were also measured to be ~29.3% at 1550 nm and ~24.2% at 1900 nm by using the homemade amplified spontaneous emission (ASE) of Er-doped gain fiber and Tm-doped gain fiber, respectively. The nonlinear optical absorption properties of microfiber-based $MoTe_2$ SA were measured by using homemade mode-locked fiber lasers with central wavelengths of 1572.4 nm (pulse duration: 642 fs, fundamental frequency: 50.12 MHz) and 1915.5 nm (pulse duration: 1.25 ps, fundamental frequency: 18.72 MHz), respectively. The nonlinear saturable absorption curves are shown in Fig. 3(b). In our experiment, the microfiber-based $MoTe_2$ SA exhibited remarkable nonlinear properties. At 1572.4 nm, the modulation depth (α_s), nonsaturable loss (α_{ns}), and saturable intensity (I_{sat}) were 25.5%, 19.1%, and 9.6 MW/cm^2, respectively. At 1915.5 nm, α_s, α_{ns}, and I_{sat} were 22.1%, 21.3%, and 12.3 MW/cm^2, respectively. The results indicated that the nonsaturable loss at 2 μm was slightly higher than that at 1.5 μm, which was caused by higher transmission loss in silica fiber at 2 μm. The modulation depths obtained at both 1572.4 nm and 1915.5 nm were about one order of magnitude larger than that of previous $MoTe_2$-based SAs [17]. The relatively large modulation depth of our microfiber-based $MoTe_2$ SA was mainly attributed to the long interaction length between the microfiber and $MoTe_2$ film. The open-aperture (OA) Z-scan technique was also carried out at 800 nm to investigate the broadband saturable absorption properties of $MoTe_2$ film. The Z-scan setup was based on a femtosecond optical parametric amplifier (OPA) that was pumped by a Ti:sapphire amplifier system. The excitation pulse duration was 100 fs with the repetition rate of 1 kHz. Figure 3(c) presents normalized OA Z-scan curves with the excitation powers of 0.4, 0.6, and 0.86 mW, respectively. The intensity-dependent transmission of the $MoTe_2$ film was clearly observed, demonstrating the effective saturable absorption of $MoTe_2$ film at 800 nm. Furthermore, pump–probe spectroscopy was also used to investigate its temporal dynamics. The excitation pulses were also from the OPA system used in the Z-scan setup. Using 400 nm degenerate pump–probe measurements, Fig. 3(d) showed the relationship between the pump-induced change of probe transmission (ΔT) and the delay time. Its dynamic relaxation process exhibited an exponential decay. The process was fitted by exponential decay function of $y = A\exp[-(x - x_0)/\tau] + y_0$, where τ represents the fast relaxation time during dynamic relaxation. The recovery time was calculated to be about 5 ps, showing the ultrafast response of the $MoTe_2$ film.

The $MoTe_2$ film was examined by X-ray diffraction (XRD) to estimate its quality. The XRD patterns were obtained by using an X'Pert Pro X-ray diffractometer (Cu Kα radiation, wavelength 1.5406 Å, 1 Å = 0.1 nm) with an operation potential of 40 kV and a current of 40 mA. As shown in Fig. 4(a), the XRD pattern of the as-prepared sample showed only peaks of pure $MoTe_2$. The peaks in the XRD pattern were assigned according to the Joint Committee on Powder Diffraction Standards (JCPDS) reference No. 73-1650 [26] with a space

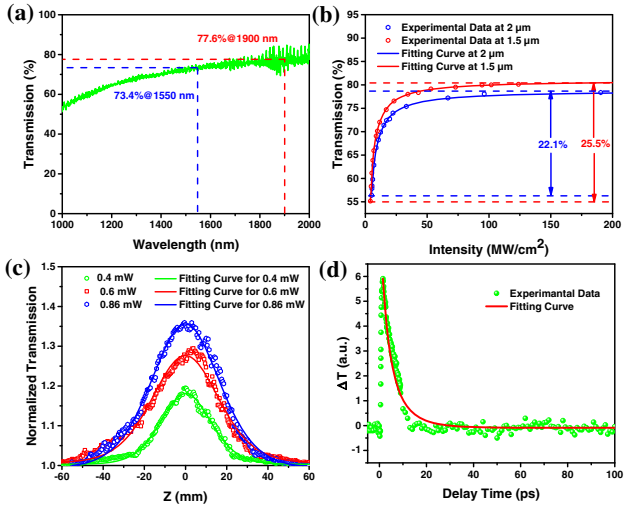

Fig. 3. (a) Linear transmission of $MoTe_2$ film. (b) Saturable absorption properties of the $MoTe_2$ SA. (c) Normalized open-aperture Z-scan traces with the excitation powers of 0.4, 0.6, and 0.86 mW, respectively. (d) Pump–probe measurement of the carrier lifetime of $MoTe_2$.

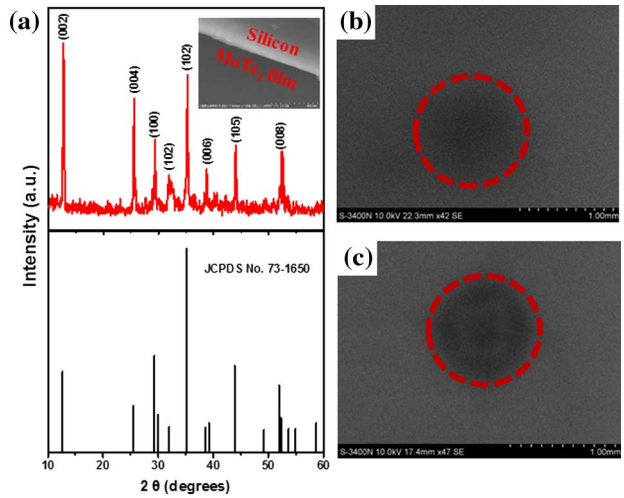

Fig. 4. (a) XRD patterns of $MoTe_2$ film. The inset shows the film quality with the scale bar of 400 nm. The SEM images with test energy densities of (b) 5.7 mJ/cm^2 and (c) 10.8 mJ/cm^2, respectively.

group of $P63/mmc$ (194). All of the observed strong and sharp peaks can be readily indexed to hexagonal α-$MoTe_2$ with lattice constants of $a = 3.52$ Å, $b = 3.52$ Å, and $c = 13.97$ Å, respectively [27]. Also, the relatively higher intensity of the (002) peak was a signature of a well-stacked layered structure [28]. The inset shows the corresponding film quality with the scale bar of 400 nm. The scratch on the film was used to distinguish the $MoTe_2$ and the substrate. The continuous and smooth surface indicated that highly uniform $MoTe_2$ film with large areas was grown by the MSD technique. The laser-induced damage threshold for $MoTe_2$ film was measured by irradiating $MoTe_2$ film grown on the Al_2O_3 substrate with the same 800 nm light source as used in the Z-scan setup. The test power was changed from 0 mJ/cm^2 to 10.8 mJ/cm^2. The damaged parts were marked with red dashed circles, as shown in Figs. 4(b) and 4(c). The optical damage of the $MoTe_2$ film appeared when the test power was 5.7 mJ/cm^2, about one order of magnitude higher than that of semiconductor saturable absorber mirrors (SESAMs) (500 μJ/cm^2) [14]. The $MoTe_2$ film was completely damaged when the test power reached 10.8 mJ/cm^2.

3. SCHEMATIC OF PASSIVELY MODE-LOCKED FIBER LASERS

The experiment setup schematic is shown in Fig. 5. For the EDF laser, a commercial 980 nm laser diode (LD) with the maximum output power of 400 mW was chosen as a pump source. A 980/1550 nm wavelength division multiplexing (WDM) coupler was used to couple the pump light into the cavity, in which a 1.5-m-long EDF [Fibercore, I-25 (980/125)] was used as the gain medium. The total cavity length was about 9.3 m. For the TDF laser, a 1550/2000 nm WDM coupler was utilized to deliver the pump light emitted by a commercial 1550 nm LD with the maximum output power of 1.4 W into the laser cavity. A piece of 3.2 m TDF (Nufern, SM-TSF-9/125) was used, and the total cavity length was about 11 m. In both fiber laser oscillators, the output coupler (OC) has a large splitting ratio of 50/50. It is in favor of extracting a large part of light out from the cavity. A polarization controller (PC) was used to adjust the state of the polarization of the oscillating beam within the cavity, and a polarization insensitive optical isolator (PI-ISO) was used to prevent back reflection in the cavity and ensure unidirectional laser operation. All components were polarization independent to avoid the self-started mode-locking operation induced by nonlinear polarization evolution (NPE). It should be noted that in both fiber laser oscillators, the direction of the operating laser was opposite to that of the pump laser so as to avoid the output of residual pump power.

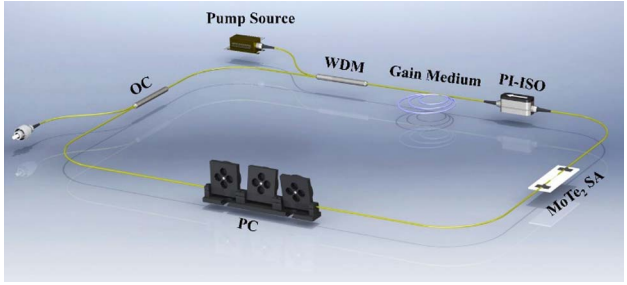

Fig. 5. Schematic of the passively mode-locked erbium- or thulium-doped fiber laser.

The characteristics of the output light were measured by an optical spectrum analyzer (Yokogawa AQ6370 for 1.5 μm, Yokogawa AQ6375B for 2 μm) and an oscilloscope (Rohde and Schwarzr RTO2024) with a photo detector (EOT ET-3500F for 1.5 μm, EOT ET-5000F for 2 μm), respectively. A radio frequency (RF) spectrum analyzer (Rohde and Schwarzr FSV13) was employed to record the RF spectrum. In addition, the pulse duration was measured by using a commercial autocorrelator (APE Pulsecheck).

4. EXPERIMENTAL RESULTS AND DISCUSSION

For our EDF laser, the self-starting mode-locking operation was observed when the pump power reached 40 mW. The mode-locking operation was stably maintained as we increased the pump power gradually. The maximum average output power was 57 mW at the pump power of 400 mW. The relationship between the pump power and output power is presented in Fig. 6(a). The output power kept a nearly linear increase with the slope of 15.4% when the pump power reached the maximum. The mode-locking performances were characterized at the maximum pump power of 400 mW. Figure 6(b) shows the typical spectrum of mode locking centered at 1559.57 nm with a 3 dB spectral bandwidth of 11.76 nm. The presence of Kelly sidebands on the spectrum confirmed that the mode-locked laser was operating in the soliton regime. The image in Fig. 6(c) shows the RF spectrum with a resolution of 10 Hz. The fundamental repetition rate was 26.601 MHz with a signal-to-noise ratio (SNR) of 93 dB, which was well matched with the cavity roundtrip time. The corresponding pulse energy is 2.14 nJ. The inset shows the RF spectrum with 1 GHz span

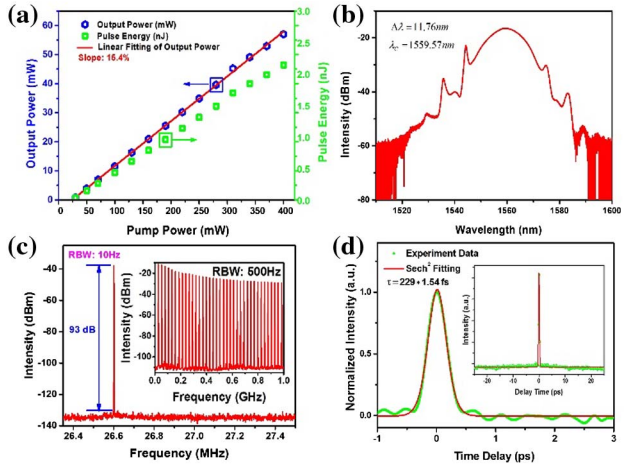

Fig. 6. Mode-locking pulse output characterizations for the EDF laser. (a) Relationship between the pump power and laser output power. (b) Optical spectrum with the bandwidth of 11.76 nm. (c) Radio frequency spectrum at fundamental frequency of 26.601 MHz with 10 Hz resolution. The inset is the RF spectrum of 1 GHz span. (d) Autocorrelation trace for output pulse with a pulse duration of 229 fs with sech^2 fit. The inset shows the autocorrelation trace with a large range of 50 ps.

under a resolution of 500 Hz, indicating the low fluctuations and the high stability of mode-locked pulse operation. The autocorrelation trace of the mode-locked pulses is shown in Fig. 6(d). The pulse duration was measured to be 229 fs. The time-bandwidth product (TBP) was calculated to be 0.332. To our knowledge, this is the shortest soliton pulse duration and highest output power among the reported values by TMDs-based SAs.

For the TDF laser, the self-starting mode-locking operation appeared at the pump power of 320 mW. As the pump power increased, the mode-locking operation remained stable even at the maximum pump power of 1.4 W. Figure 7(a) shows the power characteristic curve. The output power kept a nearly linear increase with the slope of 18.67%, and the maximum average output power was measured to be 212 mW. Figure 7(b) shows the typical output spectrum at the pump power of 1.4 W. The spectrum is centered at 1934.85 nm with a 3 dB spectral bandwidth of 3.2 nm. It is noted that the laser still operated in the soliton regime because clear Kelly sidebands were observed in the spectrum. Figure 7(c) shows the RF spectrum with a resolution of 10 Hz. The fundamental repetition rate was located at 15.37 MHz with an SNR of 84 dB, and the corresponding pulse energy was 13.8 nJ. The pulse duration, shown in Fig. 7(d), was measured to be 1.3 ps with a TBP value of 0.333. The pulse width was relatively bigger than that obtained in the EDF laser system. It can be attributed to the negative dispersion caused by both TDF (–86.8 ps^2/km at 1990 nm) and SMF (–80 ps^2/km at 1990 nm). The total group velocity dispersion was calculated to be about –0.9 ps^2, which was much larger than that in the EDF laser system.

To check the influence of the SA in our laser cavities, we replaced it by another uncoated microfiber of the same size. In that case, the mode-locking behavior could not be observed, even though the PC and the pump power were adjusted carefully. It indicated that the $MoTe_2$-SA was responsible for the mode-locked operation.

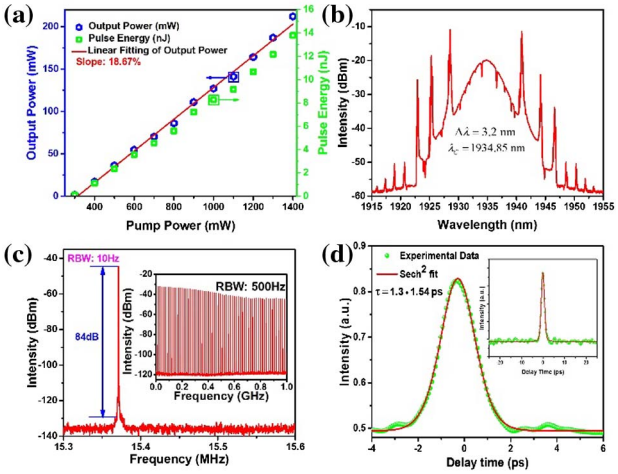

Fig. 7. Mode-locking pulse output characterizations for the TDF laser. (a) Relationship between the pump power and laser output power. (b) Optical spectrum with the bandwidth of 3.2 nm. (c) Radio frequency spectrum at fundamental frequency of 15.37 MHz with 10 Hz resolution. The inset is the RF spectrum of 1 GHz span. (d) Autocorrelation trace for output pulse with a pulse duration of 1.3 ps with $sech^2$ fit. The inset shows the autocorrelation trace with a large range of 50 ps.

It is worth mentioning that the soliton pulse wave-breaking phenomenon did not appear in either the 1.5 μm or 2 μm regime. Once the mode-locking behavior was self-starting, the laser operation was stably fixed at the fundamental frequency. The insets in Figs. 6(d) and 7(d) show the measured autocorrelation traces in a large range of 50 ps. No redundant pulse was observed, confirming that no wave-breaking phenomenon appeared in this process. Moreover, the output spectra in a large range were also measured for the two laser oscillators, and no signal was observed at the pump wavelength of 980 nm or 1550 nm. It indicated that there was no output of residual pump power for the two lasers. With the above check, the accuracy of the soliton pulse energy can be guaranteed in our experiment.

As we all know, nonlinear effects will cause wave breaking at higher energies, which leads to multiple pulse operation. According to the soliton area theorem [29], the soliton energy is inversely proportional to the average nonlinearity of a laser cavity. Compared to other reported soliton lasers by 2D materials, our laser oscillators demonstrate a great improvement of the soliton pulse energy. The high soliton energy obtained in our systems could be illustrated as follows. (i) The microfiber-based $MoTe_2$ SA with evanescent wave interaction can avoid the transmission of light through the SA material directly, which is attractive for high power tolerance. The damage threshold of the $MoTe_2$ film is as high as 5.7 mJ/cm^2 by the direct focus of high-energy testing pulses onto the film. Considering that the interaction between the light and $MoTe_2$ film is in a manner of evanescent wave interaction, the damage threshold of the $MoTe_2$ SA is expected at a higher level. Also, since the light modulation behavior appears along the whole tapered region of the microfiber, the SA would provide sufficient modulation on the lasing light in the cavity even at a high pump level. (ii) The low-doped EDF (absorption coefficient of 25 dB/m@980 nm) and TDF (absorption coefficient of 10 dB/m@1560 nm) in the experiment have large core diameters and reduced refractive indices, which are critical factors to decrease the nonlinearity in a laser cavity. (iii) The usage of the OC with high splitting ratio (50/50) in both laser cavities could also effectively reduce the intracavity nonlinearity and increase the output soliton pulse energy. It is believed that the soliton pulse energy could be further improved by optimizing the laser cavity design and the $MoTe_2$-SA properties.

For the SMFs operated in the 1.5 μm and 2 μm regimes, the latter one has a larger fundamental mode area and possesses smaller nonlinearity value [18]. Besides that, the soliton energy is proportional to the absolute value of average cavity dispersion according to the soliton area theorem [29]. The average cavity dispersion in the TDF laser (–0.9 ps^2) was much larger than that in the EDF laser (–0.12 ps^2). As a result, the mode-locked fiber lasers at 2 μm could support a higher energy soliton pulse than that obtained in the 1.5 μm fiber laser.

It is worth noting that $MoTe_2$ exhibited broadband saturable absorption at 1.5 μm (0.83 eV) and 2 μm (0.62 eV), although the photon energies were lower than its direct band gap of 1.1 eV [22]. The sub-band gap saturable absorption at

0.83 eV and 0.62 eV could be interpreted with the defect-state theory, which has been experimentally and theoretically demonstrated in other TMD nanoflakes [30,31]. For example, the broadband saturable absorption of WSe_2 has been demonstrated with the introduction of the tungsten defects [30]. The introduction of such defects in these TMDs could significantly reduce their band gaps, which are beneficial to broadband saturable absorption. In view of similar lattice structures and photonic properties for these TMDs, sub-band gap saturable absorption of $MoTe_2$ could be inferred similarly from that of WSe_2 [30] and MoS_2 [31], reported previously.

5. CONCLUSION

In conclusion, aiming to enhance the soliton pulse energy, we prepared a type of $MoTe_2$ SA with the ability of large modulation on light and high damage threshold. By applying the SA into the laser oscillators, high-energy soliton pulses were demonstrated with pulse duration/pulse energy/output power of 229 fs/2.14 nJ/57 mW in the 1.5 μm regime and 1.3 ps/13.8 nJ/212 mW in the 2 μm regime, respectively. To our knowledge, the generated soliton pulses at 1.5 μm had the shortest pulse duration and the highest output power among the reported mode-locked EDF lasers by TMDs. Moreover, the $MoTe_2$-based SA was first applied in fiber lasers in the 2 μm regime, and achieved the highest output energy of 13.8 nJ among the reported mode-locked TDF lasers by 2D materials. Our results suggest that a microfiber-based $MoTe_2$ SA could be used as an excellent photonic device for ultrafast pulse generation, and the MSD technique opens a promising route to produce high-performance SAs with large modulation depth and high power tolerance, which are beneficial for high-energy wave-breaking free pulse generation.

Funding. National Natural Science Foundation of China (NSFC) (11704260, 61405126, 61605122, 61775146); Shenzhen Science and Technology Project (JCY20150324141711695, JCYJ20160427105041864, JSGG20160429114438287, KQJSCX20160226194031, JCYJ20160422103744090); Beijing University of Posts and Telecommunications (BUPT) (IPOC2015B003); Natural Science Foundation of Guangdong Province (2016A030310049, 2016A030310059).

REFERENCES

1. R. I. Woodward and E. J. Kelleher, "2D saturable absorbers for fibre lasers," Appl. Sci. **5**, 1440–1456 (2015).
2. F. Ilday, J. Buckley, W. Clark, and F. Wise, "Self-similar evolution of parabolic pulses in a laser," Phys. Rev. Lett. **92**, 213902 (2004).
3. H. Li, H. Xia, C. Lan, C. Li, X. Zhang, J. Li, and Y. Liu, "Passively Q-switched erbium-doped fiber laser based on few-layer MoS_2 saturable absorber," IEEE Photon. Tech. Lett. **27**, 69–72 (2015).
4. Q. Bao, H. Zhang, Y. Wang, Z. Ni, Y. Yan, Z. X. Shen, K. P. Loh, and D. Y. Tang, "Atomic-layer graphene as a saturable absorber for ultrafast pulsed lasers," Adv. Funct. Mater. **19**, 3077–3083 (2009).
5. Q. Bao, H. Zhang, Z. Ni, Y. Wang, L. Polavarapu, Z. Shen, Q.-H. Xu, D. Tang, and K. P. Loh, "Monolayer graphene as a saturable absorber in a mode-locked laser," Nano Res. **4**, 297–307 (2011).
6. Z. Sun, T. Hasan, F. Torrisi, D. Popa, G. Privitera, F. Wang, F. Bonaccorso, D. M. Basko, and A. C. Ferrari, "Graphene mode-locked ultrafast laser," ACS Nano **4**, 803–810 (2010).
7. J. Wang, X. Liang, G. Hu, Z. Zheng, S. Lin, D. Ouyang, X. Wu, P. Yan, S. Ruan, and Z. Sun, "152 fs nanotube-mode-locked thulium-doped all-fiber laser," Sci. Rep. **6**, 28885 (2016).
8. J. Ma, G. Xie, P. Lv, W. Gao, P. Yuan, L. Qian, H. Yu, H. Zhang, J. Wang, and D. Tang, "Graphene mode-locked femtosecond laser at 2 μm wavelength," Opt. Lett. **37**, 2085–2087 (2012).
9. J. Sotor, G. Sobon, M. Kowalczyk, W. Macherzynski, P. Paletko, and K. M. Abramski, "Ultrafast thulium-doped fiber laser mode locked with black phosphorus," Opt. Lett. **40**, 3885–3888 (2015).
10. Y.-H. Lin, S.-F. Lin, Y.-C. Chi, C.-L. Wu, C.-H. Cheng, W.-H. Tseng, J.-H. He, C.-I. Wu, C.-K. Lee, and G.-R. Lin, "Using n- and p-type Bi_2Te_3 topological insulator nanoparticles to enable controlled femtosecond mode-locking of fiber lasers," ACS Photon. **2**, 481–490 (2015).
11. J. Koo, Y. I. Jhon, J. Park, J. Lee, Y. M. Jhon, and J. H. Lee, "Near-infrared saturable absorption of defective bulk-structured WTe_2 for femtosecond laser mode-locking," Adv. Funct. Mater. **26**, 7454–7461 (2016).
12. M. Zhang, E. J. R. Kelleher, A. S. Pozharov, E. D. Obraztsova, S. V. Popov, and J. R. Taylor, "Passive synchronization of all-fiber lasers through a common saturable absorber," Opt. Lett. **36**, 3984–3986 (2011).
13. G. H. Hu, T. Albrow-Owen, X. X. Jin, A. Ali, Y. W. Hu, R. C. T. Howe, K. Shehzad, Z. Y. Yang, X. K. Zhu, R. I. Woodward, T. C. Wu, H. Jussila, J. B. Wu, P. Peng, P. H. Tan, Z. P. Sun, E. J. R. Kelleher, M. Zhang, Y. Xu, and T. Hasan, "Black phosphorus ink formulation for inkjet printing of optoelectronics and photonics," Nat. Commun. **8**, 278 (2017).
14. H. Chen, Y. Chen, J. Yin, X. Zhang, T. Guo, and P. Yan, "High-damage-resistant tungsten disulfide saturable absorber mirror for passively Q-switched fiber laser," Opt. Express **24**, 16287–16296 (2016).
15. K. Wu, X. Zhang, J. Wang, and J. Chen, "463-MHz fundamental mode-locked fiber laser based on few-layer MoS_2 saturable absorber," Opt. Lett. **40**, 1374–1377 (2015).
16. H. Zhang, S. Lu, J. Zheng, J. Du, S. Wen, D. Tang, and K. Loh, "Molybdenum disulfide (MoS_2) as a broadband saturable absorber for ultra-fast photonics," Opt. Express **22**, 7249–7260 (2014).
17. D. Mao, B. Du, D. Yang, S. Zhang, Y. Wang, W. Zhang, X. She, H. Cheng, H. Zeng, and J. Zhao, "Nonlinear saturable absorption of liquid-exfoliated molybdenum/tungsten ditelluride nanosheets," Small **12**, 1489–1497 (2016).
18. H. Jeong, S. Y. Choi, M. H. Kim, F. Rotermund, Y. H. Cha, D. Y. Jeong, S. B. Lee, K. Lee, and D. I. Yeom, "All-fiber Tm-doped soliton laser oscillator with 6 nJ pulse energy based on evanescent field interaction with monoloayer graphene saturable absorber," Opt. Express **24**, 14152–14158 (2016).
19. J. Boguslawski, G. Sobon, R. Zybala, and J. Sotor, "Dissipative soliton generation in Er-doped fiber laser mode-locked by Sb_2Te_3 topological insulator," Opt. Lett. **40**, 2786–2789 (2015).
20. P. Yan, H. Chen, J. Yin, Z. Xu, J. Li, Z. Jiang, W. Zhang, J. Wang, I. L. Li, and Z. Sun, "Large-area tungsten disulfide for ultrafast photonics," Nanoscale **9**, 1871–1877 (2017).
21. J. Wang, S. Lin, X. Liang, M. Wang, P. Yan, G. Hu, T. Albrow-Owen, S. Ruan, Z. Sun, and T. Hasan, "High-energy and efficient Raman soliton generation tunable from 1.98 to 2.29 μm in an all-silica-fiber thulium laser system," Opt. Lett. **42**, 3518–3521 (2017).
22. C. Ruppert, O. B. Aslan, and T. F. Heinz, "Optical properties and band gap of single- and few-layer $MoTe_2$ crystals," Nano Lett. **14**, 6231–6236 (2014).
23. P. Tonndorf, R. Schmidt, P. Böttger, X. Zhang, J. Börner, A. Liebig, M. Albrecht, C. Kloc, O. Gordan, D. R. T. Zahn, S. Michaelis de Vasconcellos, and R. Bratschitsch, "Photoluminescence emission and Raman response of monolayer MoS_2, $MoSe_2$, and WSe_2," Opt. Express **21**, 4908–4916 (2013).
24. L. Zhou, K. Xu, A. Zubair, X. Zhang, F. P. Ouyang, T. Palacios, M. S. Dresselhaus, Y. F. Li, and J. Kong, "Role of molecular sieves in the CVD synthesis of large-area 2D $MoTe_2$," Adv. Funct. Mater. **27**, 1603491 (2017).
25. J. H. Huang, K. Y. Deng, P. S. Liu, C. T. Wu, C. T. Chou, W. H. Chang, Y. J. Lee, and T. H. Hou, "Large-area 2D layered $MoTe_2$ by physical vapor deposition and solid-phase crystallization in a tellurium-free atmosphere," Adv. Mater. Interfaces **4**, 1700157 (2017).

26. O. Knop and R. D. MacDonald, "Chalkogenides of the transition elements: III. Molybdenum ditelluride," Can. J. Chem. **39**, 897–904 (1961).
27. L. H. Qiu, Y. Wei, V. G. Pol, and A. Gedanken, "Synthesis of alpha-$MoTe_2$ nanorods via annealing Te-seeded amorphous $MoTe_2$ particles," Inorg. Chem. **43**, 6061–6066 (2004).
28. A. Roy, H. C. P. Movva, B. Satpati, K. Kim, R. Dey, A. Rai, T. Pramanik, S. Guchhait, E. Tutuc, and S. K. Banerjee, "Structural and electrical properties of $MoTe_2$ and $MoSe_2$ grown by molecular beam epitaxy," ACS Appl. Mater. Interfaces **8**, 7396–7402 (2016).
29. C. S. Jun, S. Y. Choi, F. Rotermund, B. Y. Kim, and D. I. Yeom, "Toward higher-order passive harmonic mode-locking of a soliton fiber laser," Opt. Lett. **37**, 1862–1864 (2012).
30. J. Yin, J. Li, H. Chen, J. Wang, P. Yan, M. Liu, W. Liu, W. Lu, Z. Xu, W. Zhang, J. Wang, Z. Sun, and S. Ruan, "Large-area highly crystalline WSe_2 atomic layers for ultrafast pulsed lasers," Opt. Express **25**, 30020–30031 (2017).
31. M. Trushin, E. J. R. Kelleher, and T. Hasan, "Theory of edge-state optical absorption in two-dimensional transition metal dichalcogenide flakes," Phys. Rev. B **94**, 155301 (2016).